# UC Berkeley
## UC Berkeley Previously Published Works

**Title**

Quantitative evaluation of the feasibility of sampling the ice plumes at Enceladus for biomarkers of extraterrestrial life

**Permalink**

**Journal**

Proceedings of the National Academy of Sciences of the United States of America, 118(37)

**ISSN**

0027-8424

**Authors**

New, James S
Kazemi, Bahar
Spathis, Vassilia
et al.

**Publication Date**

2021-09-14

**DOI**

10.1073/pnas.2106197118

Peer reviewed

# Quantitative evaluation of the feasibility of sampling the ice plumes at Enceladus for biomarkers of extraterrestrial life

James S. New[a,b] , Bahar Kazemi[c] , Vassilia Spathis[b] , Mark C. Price[b], Richard A. Mathies[a,c] , and Anna L. Butterworth[a,1]

[a]Space Sciences Laboratory, University of California, Berkeley, CA 94720; [b]School of Physical Sciences, University of Kent, Kent CT2 7NH, United Kingdom; and [c]Department of Chemistry, University of California, Berkeley, CA 94720

Enceladus, an icy moon of Saturn, is a compelling destination for a probe seeking biosignatures of extraterrestrial life because its subsurface ocean exhibits significant organic chemistry that is directly accessible by sampling cryovolcanic plumes. State-of-the-art organic chemical analysis instruments can perform valuable science measurements at Enceladus provided they receive sufficient plume material in a fly-by or orbiter plume transit. To explore the feasibility of plume sampling, we performed light gas gun experiments impacting micrometer-sized ice particles containing a fluorescent dye biosignature simulant into a variety of soft metal capture surfaces at velocities from 800 m · s$^{-1}$ up to 3 km · s$^{-1}$. Quantitative fluorescence microscopy of the capture surfaces demonstrates organic capture efficiencies of up to 80 to 90% for isolated impact craters and of at least 17% on average on indium and aluminum capture surfaces at velocities up to 2.2 km · s$^{-1}$. Our results reveal the relationships between impact velocity, particle size, capture surface, and capture efficiency for a variety of possible plume transit scenarios. Combined with sensitive microfluidic chemical analysis instruments, we predict that our capture system can be used to detect organic molecules in Enceladus plume ice at the 1 nM level—a sensitivity thought to be meaningful and informative for probing habitability and biosignatures.

planetary exploration | ocean worlds | ice particle impacts | astrobiology | space sciences instrumentation

Saturn's moon Enceladus is an ideal location to search for molecular signs of extraterrestrial life within our solar system (1–3). Spectacular water vapor and ice plumes jet into space (4, 5) from a subsurface ocean through cracks in its frozen ice surface (6, 7) providing pristine samples available for analysis. First discovered by the Cassini–Huygens mission in 2005, the plumes are associated with plentiful evidence of habitability: the presence of a rocky core (8), hydrothermal activity at the ocean-core boundary (9–11), geochemical processes (12), and the presence of simple organic compounds (13, 14) as well as complex macromolecular organics (15, 16), which may be present as a thin organic-rich film on top of the oceanic water table. Enceladus therefore satisfies established criteria for habitability, including the presence of liquid water, a source of energy, and organic chemicals that are potential building blocks of life. Cassini's rich data set provides tantalizing clues to the prevalence and complexity of carbon chemistry deep in Enceladus. These observations justify the development and use of high-performance liquid phase microfluidic organic analysis instruments (17–19) to probe the Enceladus ocean for habitability and for potential biosignatures by analyzing the trace chemical composition of plume ice particles in more sensitive and high-resolution detail.

Neveu et al. recently presented a comprehensive review of the possible mission formats and considerations for sampling the Enceladus plume (20). A critical step in designing a mission for trace organic biosignature detection from the plume is developing and deploying a capture system that efficiently gathers intact organic molecules while passing through the plume (21) at velocities from a few hundred m · s$^{-1}$ to 3 km · s$^{-1}$. It is important

to evaluate capture surfaces (CSs) at a variety of velocities representing the relative encounter of a spacecraft transecting with plume ice particles. Because capture efficiency is expected to vary with particle size (22) another challenge is ensuring that the experimental ice particle projectile size range encompasses the Enceladus plume brine ice particle sizes (median radius ∼3 μm) that contribute the most mass density to the plume.

To address these challenges, we have evaluated the high-velocity capture of organic doped ice particles, 2 to 10 μm in diameter, utilizing soft metal CSs including Al, Au, and In with mechanical and thermal properties chosen to optimize ice capture and organic survival (18). The idea is to optimize capture efficiency, for a particular particle size-range and encounter velocity, by selecting a CS that is compliant to minimize shock disruption and has high thermal conductivity to minimize ice impact heating. The metals studied were chosen to have low reactivity to avoid catalyzing unwanted compositional changes. The CS must be fabricated and maintained to meet stringent cleanliness requirements for planetary protection, limiting trace organic contamination to parts per trillion levels. The CS must also permit complete release of any captured organics for subsequent liquid phase chemical analysis. For example, Al foil collectors were previously deployed in NASA's Stardust mission to collect cometary dust, with evidence that traces of entrained amino acids survived the 6.1 km·s$^{-1}$ impact speed (23, 24).

Proper evaluation of a capture system requires that experiments quantitatively and realistically represent organic ice particle capture

## Significance

The search for organic biosignatures indicative of life elsewhere in our solar system is an exciting quest that, if successful, will have a profound impact on our biological uniqueness. Saturn's icy moon Enceladus is a promising location for a second occurrence of life due to its salty subsurface ocean. Plumes that jet out through the ice surface vents provide an enticing opportunity to sample the underlying ocean for biomarkers. The experiments reported here provide accurate modeling of our ability to fly through these plumes to efficiently and nondestructively gather ice particles for biomolecular analysis. Our measured efficiencies demonstrate that Saturn and/or Enceladus orbital missions will gather sufficient ice to make meaningful measurement of biosignatures in the Enceladus plumes.

in high-velocity impacts. The "cold" light gas gun (LGG) at the University of Kent, United Kingdom (25, 26), has the ability to perform high-precision, high-velocity shots of particles including ice into targets. Initial studies with poly(methyl-methacrylate) monodisperse microparticle projectiles revealed the relationship between crater size and impacting particle size and velocity for our CS materials (22). This result was needed to quantitate the size of impacting ice particles based on crater size for a distribution of ice fragment sizes produced in an ice shot. Next, we developed and tested a method of freezing ice projectiles doped with organic tracers and firing them at high velocities into targets of interest (27). In the LGG, the rapid acceleration to velocities up to 3.0 km · s$^{-1}$ shatters the solid ice projectile, resulting in a wide distribution of micrometer-sized brine ice particle fragments that hit the CS, encompassing the range of particle sizes expected in the Enceladus plume (28), but does not include the smaller water ice particles formed through homogeneous nucleation from water vapor (6), which are less relevant to biosignature searches. Finally, a calibrated epifluorescence microscope method was developed using a fluorescent tracer dye, Pacific Blue (PB), for quantifying the amount of unmodified organic molecules detected on a CS target on a crater-by-crater basis (29). With these calibration experiments in hand, the stage was set for experiments that accurately represent ice impacts in an Enceladus plume encounter.

The results presented here allow us to quantitate the organic capture efficiency with respect to impact velocity and particle size in a range that is relevant for a variety of Enceladus plume transits. Combining the quantitative evaluation of the performance of our CS materials with the sensitive analysis capabilities of microfluidic chemical analysis instruments with laser-induced fluorescence (LIF) detection allows us to predict the science measurement potential of a variety of Enceladus plume sampling mission formats. Based on these calculations, we find that there are several scenarios that can provide highly meaningful information about organic chemical signatures of habitability and possible extraterrestrial life at Enceladus.

## Results

We analyzed over 1,200 craters formed by high-velocity ice particle impacts into soft metal foils using epifluorescence microscopy to quantitate the amount of the PB fluorescent dye in each crater. Using the crater-size to particle-size calibrations and fluorescence intensity calibrations determined earlier (27, 29), we explored the relationship between organic capture efficiency, impact velocity (0.8 to 3.0 km · s$^{-1}$), CS material, and ice-particle size (2 to 30 μm in diameter).

Fig. 1 presents an overview of our results with organic capture efficiency plotted against impact velocity; particle size bins are distinguished by marker color. The large number of markers extending to over 20% capture efficiencies in the upper left region of the indium plot at velocities ≤1.7 km · s$^{-1}$ indicates that indium is the optimum CS material for low-velocity impacts. The large number of markers above 20% capture efficiency in the upper right region of the aluminum plot at 2.2 and 2.7 km · s$^{-1}$ shows that, at higher impact velocities, the aluminum CS is most effective. Gold exhibited significantly lower capture efficiencies at all velocities and particle sizes. The consistency of the PB emission spectrum up to the 3 km · s$^{-1}$ velocities studied indicates that the reduced capture efficiency is primarily due to physical particle loss.

Fig. 1 highlights the relationship between particle size and capture efficiency for each impact velocity and CS material. The highest capture efficiency regions for each velocity on the indium and aluminum plots are predominantly populated with red markers that represent 1 to 10 μm diameter particles that are most relevant for Enceladus. This indicates that, for both In and Al CS materials at all velocities, capture efficiency is higher for
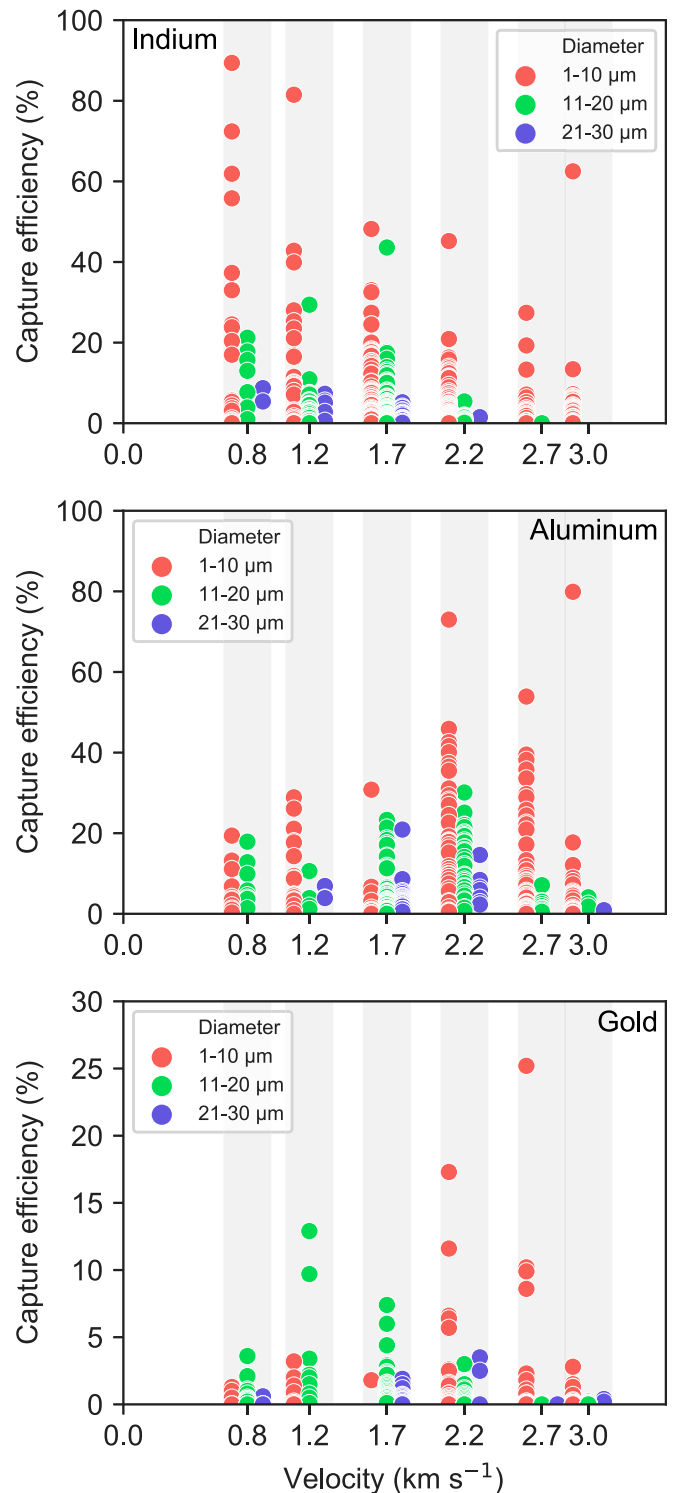


**Fig. 1.** Capture efficiency (%) plotted against shot velocity (km · s$^{-1}$) for impacts on In, Al, and Au capture surfaces at velocities ranging from 0.8 to 3.0 km · s$^{-1}$. The individual particles are shown in size bins: (Red) 1 to 10 μm, (Green) 11 to 20 μm, and (Blue) 21 to 30 μm. Each shot velocity was uniform for all particle sizes across all three target materials; the markers are spread horizontally for visual clarity. The low capture efficiencies on Au are displayed with the y-axis capped at 30. The large variation in capture efficiency is likely due to differences in particle fragment morphology.

smaller particles. Larger 11 to 20 μm diameter particles (green) are captured with relatively high efficiency for velocities below 2.0 km · s$^{-1}$ on indium and below 2.5 km · s$^{-1}$ on aluminum.
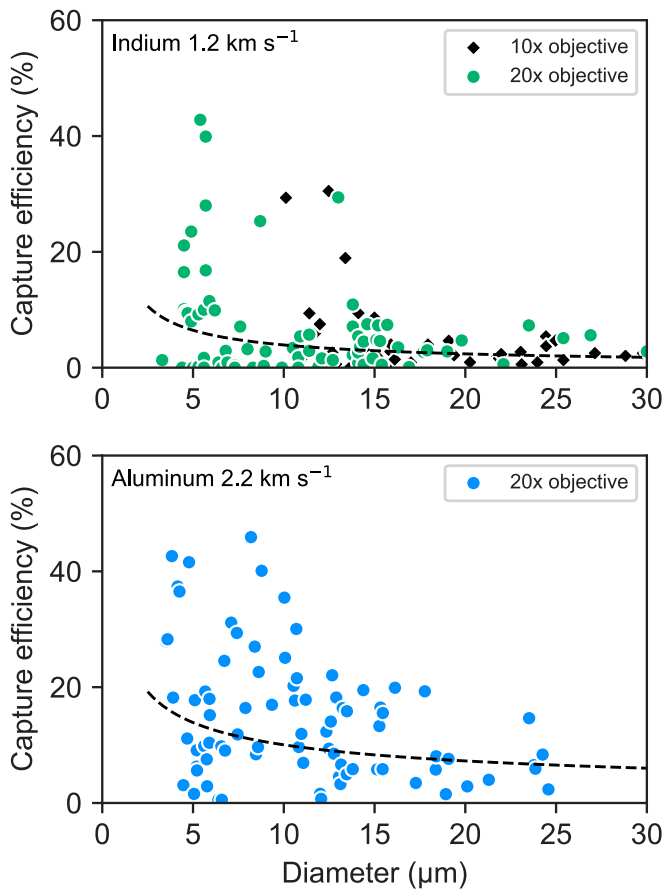
**Fig. 2.** Capture efficiency (%) plotted against particle diameter (μm) and fit to a 1/diameter dependence. The indium plot presents 1.2 km · s⁻¹ velocity data where the green dots represent measurements made using a 20× objective lens and black diamonds represent data collected using a 10× objective apparatus from ref. 27. The best fit line for the combined data set is $y = 20.5x^{-0.72}$. The aluminum plot presents 2.2 km · s⁻¹ velocity impact data collected using a 20× objective lens with a best fit line $y = 29.5x^{-0.47}$.

Fig. 2 plots capture efficiency against particle diameter for impacts at optimum capture velocities on indium (1.2 km · s⁻¹) and aluminum (2.2 km · s⁻¹). For comparison, the indium plot includes previously collected data (black diamonds) (27) and new data (green dots). These data are fit to 1/diameter because we expect capture to qualitatively scale with the ratio of particle surface area/volume, as discussed previously (22). The fit confirms our earlier suggestion (27) that capture efficiencies increase for smaller ice particles, consistent with the 1/diameter function. Smaller particles (d < 10 μm) are captured with high efficiency with half of the events over 10%, while the larger particles have an upper capture limit of 10%. The aluminum plot demonstrates a similar relationship between capture efficiency and particle size with a higher population of impacts exhibiting capture efficiency above 20% for <10 μm particles. As particle size increases (d > 10 μm), the capture efficiency falls below 20%. For both indium and aluminum, capture efficiencies as high as 80 to 90% are observed for individual impact events involving especially small (d < 5 μm) particles.

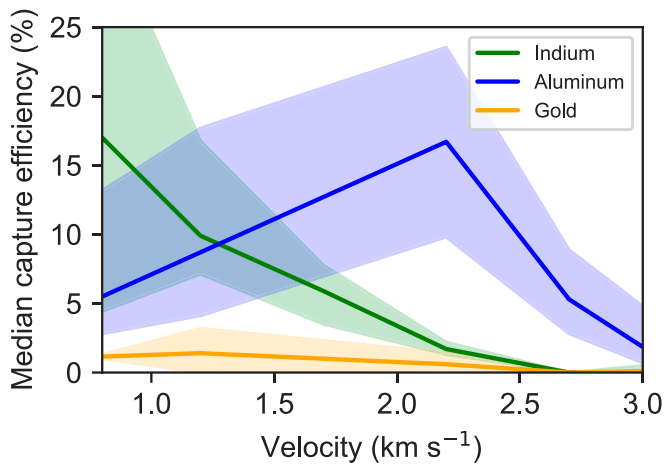Fig. 3 compares capture efficiency results for each CS for particles ≤10 μm in diameter. Indium is the most effective CS material for low velocities (v < 1.7 km · s⁻¹) with the median capture efficiencies ranging from 5.6 to 7.1%. Capture efficiencies on indium for individual impacts (excluding outliers) range up to 62 ± 16%, 28 ± 7%, and 27 ± 7% at 0.8, 1.2, and 1.7 km· s⁻¹, respectively. At higher velocities (v ≥ 2.2 km · s⁻¹) aluminum is the most effective CS material with median capture efficiencies of

17 ± 4%, 5 ± 1%, and 2 ± 0.5% at velocities of 2.2, 2.7, and 3.0 km · s⁻¹, respectively. Capture efficiencies for individual impacts (excluding outliers) reached 46 ± 12%, 40 ± 10%, and 12 ± 3% across the same velocity intervals. In contrast, the median capture efficiency on indium falls below 0.1% at velocities greater than 2.2 km · s⁻¹.

Summary Fig. 4 plots median capture efficiencies, with 95% CI bands, against velocity for each CS material. Craters with capture consistent with background noise (≤0.5%) are removed for velocities ≤ 1.2 km · s⁻¹ to account for particles that remain intact and fall off the vertical target surface due to gravity. At low velocities (v < 1.2 km · s⁻¹), indium exhibits the highest capture efficiency that rises strongly from 10 to 17% at the slowest velocity studied. Above 1.2 km · s⁻¹ aluminum is the most effective CS material; its capture efficiency rises to 17 ± 4% at 2.2 km · s⁻¹ and then drops to 2 ± 0.5% at 3.0 km · s⁻¹.
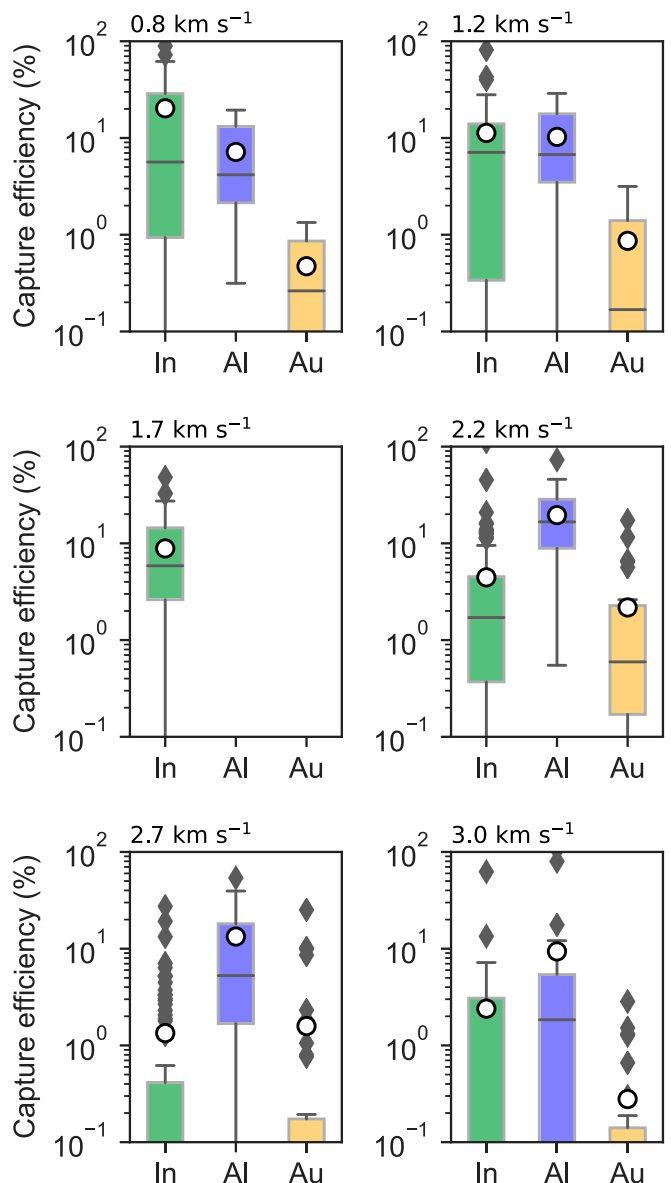
**Fig. 3.** Capture efficiency (%) for small (d ≤ 10 μm) particles impacting In (green), Al-1100 (blue), and Au (gold) capture surfaces with velocities between 0.8 and 3.0 km · s⁻¹. The results include the median (central line), mean (hollow circle), interquartile range (IQR), and outliers (diamonds) based on Tukey's method (1.5 IQR inclusive median).

New et al.
Quantitative evaluation of the feasibility of sampling the ice plumes at Enceladus for biomarkers of extraterrestrial life

PNAS | 3 of 6
https://doi.org/10.1073/pnas.2106197118

**Fig. 4.** Median capture efficiency (%) for small (d ≤ 10 μm) particles representative of Enceladus plume particles, with 95% confidence bands plotted against velocity (km · s⁻¹) for indium (green), aluminum (blue), and gold (gold) capture surfaces.

## Discussion

The search for organic molecules, biosignatures, and the possible presence of extraterrestrial life in our solar system is an exciting quest that, if successful, will have a profound impact on our understanding of our biological uniqueness (30). Our research addresses the challenges of developing scientific and engineering approaches for high-sensitivity solar system sampling for bio-organic signatures while addressing planetary protection by establishing the feasibility of missions that do not contact the moon surface. Such missions include a Saturn orbiter that makes close 2 km · s⁻¹ and higher velocity passes to Enceladus' south pole to interrogate the plumes (31). The alternative Enceladus orbiter format would involve much lower relative speeds of around 200 m · s⁻¹ because of the small size of the moon.

We have developed and evaluated soft metallic CSs that enable high-efficiency nondestructive organic molecule capture in an ice plume fly-by or orbiter mission format. Frozen ice projectiles containing a fluorescent organic tracer molecule were fired at CS targets at high velocities using the "cold" LGG at Kent. Organic capture on each CS was measured by quantitative fluorescence microscopy of individual craters corresponding to 2 to 30 μm in diameter particle sizes (22, 27, 29).

The most important results for evaluating possible Enceladus missions are summarized in Fig. 4, which focuses on the median capture efficiency for ice particles ≤10 μm in diameter on Al, In, and Au targets. The softest metal surfaces (i.e., indium) are ideal for low velocity (≤1.2 km · s⁻¹) impacts providing the highest measured median capture efficiency of at least $17 \pm 4\%$ at 0.8 km · s⁻¹ when integrated over a large number of impacts. At low velocities, particles remain intact and likely stick to the soft CS but are potentially undercounted in these experiments due to gravity overcoming weakly adhered particles on vertically mounted foil targets; data points in Fig. 2 of impact craters with zero capture provide our best estimate of this process. The trend in Fig. 4 and experimental fits to the capture efficiency for small particles as a function of velocity predict capture efficiency increasing as the velocity decreases below 800 m · s⁻¹. Thus, the measured 17% efficiency on the softest CS should be applicable to lower velocities that are appropriate for an Enceladus orbiter.

At higher velocity (≥1.2 km · s⁻¹), a median capture efficiency of $17 \pm 4\%$ was achieved with the harder aluminum target, with capture peaking at 2.2 km · s⁻¹ and still significant at 3 km · s⁻¹, approaching Enceladus plume encounter speeds for a Saturn orbit profile. At these velocities, the ice particles likely melt on

impact (22). Gold did not capture organic-doped ice particles efficiently compared to the previous successful capture of poly-methylmethacrylate (PMMA) ice analogs on Au at 1 to 2 km · s⁻¹ (22). This result indicates the challenge of using ice models in impact studies and the need for direct ice impact experiments.

Quantitatively estimating the amount of ice gathered by a particular CS requires consideration of impact velocity and particle size range that in turn depends on fly-by closest approach distance through Enceladus' plume; particles are expected to be larger at lower altitudes in the plume (21, 32, 33). This is quantitatively illustrated in Fig. 5, which shows that the total volume of captured ice increases rapidly with particle size despite the dramatic reduction in capture efficiency with particle size. This makes sense because the capture area scales as the diameter squared while the particle volume scales as the cube (22). For 2.2 km · s⁻¹ impacts onto aluminum, particles from 1 to 5 μm diameter are captured at 17% efficiency resulted in $7 \times 10^{-3}$ pL captured per particle on average. However, larger ice particles shot in the same experiment with diameters from 21 to 25 μm are captured at only ~2% efficiency but provide a dramatic increase to 0.5 pL captured per particle. Thus, lower elevation transits through the Enceladus plume to capture larger particles may be advantageous for biomarker sampling despite the lower capture efficiency for larger particles.

The ice particle size and particle density at the closest approach through the plume are critical inputs to the calculation of the total amount of ice harvested, presented as volume of ice encountered per area of a plume transect at a given altitude. Higher plume particle densities are spatially associated with the surface vents (34). While the bulk plume emission rate of 200 to 1,000 kg · s⁻¹ (35) of mostly water vapor was stable to within 15% over 6 y of Cassini observations, temporal variations in plume density have been detected (33). In particular, ice particle production from the vents varies due to diurnal tidal stresses from Saturn (36). Particle size and density also vary with altitude, as small particles (<3 μm in radius) can exceed Enceladus' escape velocity of ~250 m · s⁻¹ to be ejected into Saturn's E-ring (5). Larger particles emitted at slower speeds as frozen aerosol spray (32) may decouple from the venting supersonic gas jets and fall back to the moon's surface (37). The density of particles is proportional to altitude ($z^{-1/3}$) (33) although there are uncertainties due to whether ice particles are considered as dense spheres or as low-density aggregates (38). Based on these observations one transect of Enceladus' plume, at the same nominal 50 km fly-by
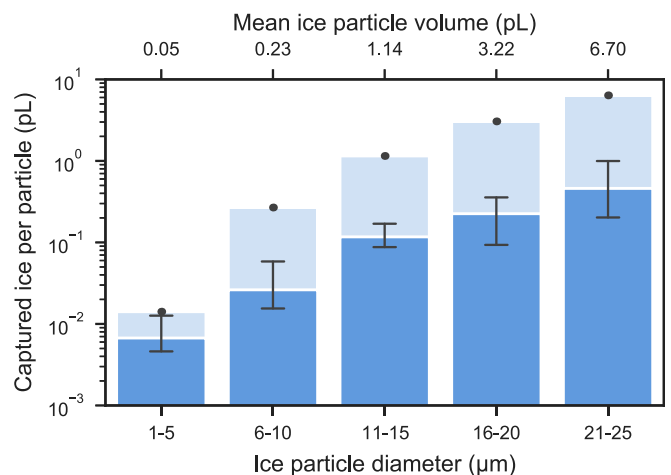


**Fig. 5.** Capture efficiency and particle size: the mean capture volume (pL) per particle plotted against particle diameter and mean volume for impacts on Al at 2.2 km · s⁻¹. The dark blue bars represent volume captured, and the light blue bars represent 100% capture. 95% CIs are depicted by the black markers.

altitude as Cassini, is expected to gather ~2 µL · m$^{-2}$ (within an expected range 1 to 5 µL · m$^{-2}$) of ice particles with a diameter less than 10 µm for analysis (39).

The final piece of information needed to evaluate approaches for high-sensitivity solar system plume sampling is what sensitivity is necessary to make a meaningful biosignature measurement? The Europa Lander Science Definition Team selected a target science measurement goal of 1 nM in the extraterrestrial sample for that proposed mission (40), based on low cell density terrestrial ecosystems that harbor extremophiles (41). Useful terrestrial comparisons are deep aphotic polar oceans; deep, cold brines; and subglacial liquid water environments (e.g., Lake Vostok, Lake Vida and winter circumpolar deep water) where reported concentrations of dissolved free amino acids are in the 1 to 200 nM range (42–44). Based on these same observations, we adopt the 1 nM biosignature terrestrial reference state as the definition of a meaningful measurement level for discussion, realizing that life at its extreme limits may exhibit lower biosignature levels.

We now quantitatively evaluate the science measurement capabilities of several mission profiles for sampling the Enceladus plumes and predict the scientific utility. With our experimentally determined 17% average organic capture efficiency, a CS of 1 m$^2$ area will accumulate 0.34 µL of ice in one transit. Solution-based analytical methods require that species be dissolved into a small volume for chemical analysis because the detection limits are determined by the analyte molar concentration. A 10 µL analytical volume is typical in microfluidic applications, sufficient for fluid dissolution, transport, and manipulation (45). In this example, an amino acid biomarker present in the Enceladus plume ice at 1 nM concentration would be captured in the equivalent of 0.34 µL ice in a single plume pass, dissolved into 10 µL solution, resulting in a concentration of 34 pM at the detector (assuming 100% dissolution). LIF detection in capillary systems has for decades been capable of 10 pM detection limits extending to 100 fM or below with more exotic detection approaches (46–48). Prototype biosignature detection apparatus, initially developed for analysis of amino acids at Mars, has demonstrated from 75 to 100 pM detection limits that are very close to the desired sensitivity (17, 49). Our more recent work developing a microfluidic organic analyzer in a flight-ready format has extended this sensitivity limit to the ~30 pM level (18, 50, 51). Note that this sensitivity can be achieved through a low-velocity pass using an Enceladus orbiter, but similar results can be expected in the 1 to 3 km· s$^{-1}$ range that are more consistent with a Saturn orbit (52). Thus, a mission probing the Enceladus plume has the potential for a meaningful science measurement relative to the terrestrial reference state.

While this is an encouraging result, there are a number of improvements that can further enhance the projected science measurement capabilities. For a concentration-based experiment, the sensitivity and/or ability to perform additional confirmatory experiments can be increased by collecting more sample by making multiple plume passes. For example, using an Enceladus periodic orbit (53), it would easily be possible for a spacecraft to make 10 passes through the plume or more. Ten passes would collect tenfold more sample (3.4 µL m$^2$ of ice in a 1 m$^2$ collector), which, if dissolved into the same 10 µL analysis volume, would present a readily detectable biosignature concentration of 340 pM starting from 1 nM in the input ice sample. Multiple passes are also feasible with Saturn orbiter profiles (31). Multiple passes are also advantageous to compensate for spatial and temporal variations in the plume density and location (33, 54). Lower altitude plume transects with higher densities and larger plume ice particles (33) could also be employed to enhance sample collection, resulting in better detection limits (21). Finally, Mathies et al. recently presented approaches to modify the CS surface to enhance capture efficiency beyond the useful levels demonstrated here as well as microfabricated surfaces that facilitate analyte dissolution in a small useful volume (55). With combined improvements in measurement sensitivity

possible from gathering additional samples through more passes and or at lower trajectories, increased capture efficiency, and improved sample transport efficiency, a single spacecraft collector could support multiple complementary instruments in either an in situ Enceladus orbiter or Saturn orbiter format. Our results on capture methodology coupled with these potential improvements would also enhance the capabilities of an Enceladus sample return mission (20).

In conclusion, we have developed and validated capture surfaces that efficiently gather organic-containing ice particles in high-velocity encounters using an experimental approach that accurately models an Enceladus ice plume encounter. The quantitative measurement of capture efficiencies allows us to more accurately assess whether an Enceladus mission can be used to perform a valid comparison of biosignatures in relation to our one available reference state—Earth. Importantly, the ice capture system at encounter velocities up to 3 km · s$^{-1}$ provides efficient sampling of intact native organic signatures in quantities that enable biosignature detection approaching the 1 nM level or better. This is the level thought to be meaningful and informative for habitability and biosignature measurements. Thus, Enceladus plume sampling missions searching for extraterrestrial biosignatures can provide high science return, reduce planetary protection challenges, and lower risk and expense compared to landed missions.

## Materials and Methods

The "cold" LGG at the University of Kent, United Kingdom (25, 26), schematized in Fig. 6A was used to fire organic doped ice projectiles into vertical metal foil targets. A detailed description of the LGG experimental setup and procedure is available (27). Briefly, PB stock solution (10 mM) was diluted in a sodium tetraborate buffer solution (30 mM [pH 9.5]) and frozen (−25 °C) into 90 mm$^3$ cylindrical projectiles (PB final concentration 100 µM) as seen in Fig. 6. The shot procedure begins when a shotgun cartridge detonates, driving a piston that compresses a light gas in the pump tube. When the gas reaches a chosen pressure, a thin burst disk ruptures, and the compressed gas is released rapidly accelerating the ice projectile through a frozen (−100 °C) and evacuated (50 mbar) launch tube. The sudden acceleration causes the ice to fragment, creating a plume of small (micrometers to millimeters in diameter) ice particles (Fig. 6B) that proceed through the evacuated blast tank and impact the vertical-mounted foil targets. The velocity is accurately measured (±0.05 km · s$^{-1}$) via laser
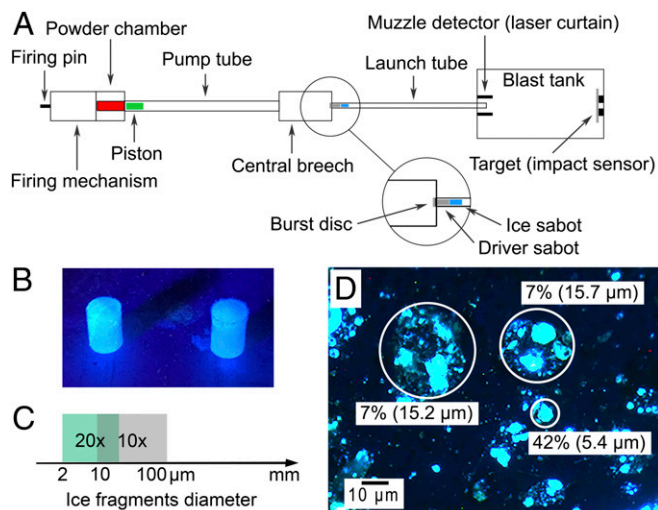


**Fig. 6.** (A) Schematic of the LGG experiment. (B) Doped ice sabot projectiles (90 µL), shown illuminated by UV light, shatter during acceleration producing a spray of fragments that impact the target. (C) Ice fragments range from microns to millimeters in diameter. Thus, two sets of microscope objectives and humidifying apparatus were optimized for analyzing particle/craters in the 2 to 30 and 10 to 100 µm diameter range shaded in green (20× objective) and gray (10× objective), respectively. (D) Representative craters circled, with PB residue (blue) fluorescing under UV light under 70% ambient humidity. Capture efficiencies and crater diameters are indicated.

New et al.
Quantitative evaluation of the feasibility of sampling the ice plumes at Enceladus for biomarkers of extraterrestrial life

PNAS | 5 of 6
https://doi.org/10.1073/pnas.2106197118

curtains and impact sensors positioned on the target. Impact experiments were carried out at velocities of 0.8, 1.2, 1.7, 2.2, 2.7, and 3.0 km $\cdot$ s$^{-1}$ on foil targets composed of high purity, soft Al (Al-1100), Au and In (all from Goodfellow).

PB ($C_{10}H_4F_2O_7$, molecular mass: 274, Thermo Fisher Scientific) is an organic fluorophore that was selected to quantify the capture of intact organic molecules by measuring the fluorescence in the impact craters. Organic capture was calculated as the ratio between the number of PB molecules captured on the foil and the number of PB molecules in the impacting particle.

An epifluorescence microscope with a mercury light source was used to illuminate the foils and detect PB emission. Three images were taken of each crater: a bright-field image to identify and select craters; a humidified (70%) UV image to identify and quantify the PB molecular residues presented in Fig. 6D; and a dehumidified UV image to identify fluorescent artifacts and subtract background. The volume of ice in each impact was calculated using the crater dimensions measured in ImageJ (56) and the crater-size to particle-size calibration (22). The number of PB molecules in each ice particle was derived from the ice volume and initial concentration of PB. The number of PB molecules deposited in each crater was measured using fluorescence intensity calibrations. Detailed descriptions of the microscope, analysis method, and fluorescence calibration are available in ref. 29.

The observed variation in capture efficiency for a given velocity and particle size is most likely due to random variations in particle morphology away from a spherical shape which leads to an underestimate in captured ice volume and hence lower PB capture. Furthermore, some particles that would otherwise adhere are lost in our experiments due to the vertical orientation of our targets in a gravitational field. Thus, our capture percentages are likely underestimates of the true values.

1. J. I. Lunine, Ocean worlds exploration. *Acta Astronaut.* **131**, 123–130 (2017).
2. K. P. Hand, C. Sotin, A. Hayes, A. Coustenis, On the habitability and future exploration of ocean worlds. *Space Sci. Rev.* **216**, 1–24 (2020).
3. M. L. Cable et al., The science case for a return to Enceladus. *Planet. Sci. J.* **2**, 132 (2021).
4. C. C. Porco et al., Cassini observes the active south pole of Enceladus. *Science* **311**, 1393–1401 (2006).
5. F. Spahn et al., Cassini dust measurements at Enceladus and implications for the origin of the E ring. *Science* **311**, 1416–1418 (2006).
6. F. Postberg et al., Sodium salts in E-ring ice grains from an ocean below the surface of Enceladus. *Nature* **459**, 1098–1101 (2009).
7. J. H. J. Waite et al., Liquid water on Enceladus from observations of ammonia and 40Ar in the plume. *Nature* **460**, 487–490 (2009).
8. L. Iess et al., The gravity field and interior structure of Enceladus. *Science* **344**, 78–80 (2014).
9. H.-W. Hsu et al., Ongoing hydrothermal activities within Enceladus. *Nature* **519**, 207–210 (2015).
10. Y. Sekine et al., High-temperature water-rock interactions and hydrothermal environments in the chondrite-like core of Enceladus. *Nat. Commun.* **6**, 8604 (2015).
11. J. H. Waite et al., Cassini finds molecular hydrogen in the Enceladus plume: Evidence for hydrothermal processes. *Science* **356**, 155–159 (2017).
12. C. R. Glein, M. Y. Zolotov, Hydrogen, hydrocarbons, and habitability across the solar system. *Elements* **16**, 47–52 (2020).
13. F. Postberg et al., The E-ring in the vicinity of Enceladus II. Probing the moon's interior—The composition of E-ring particles. *Icarus* **193**, 438–454 (2008).
14. J. H. J. Waite Jr et al., Cassini ion and neutral mass spectrometer: Enceladus plume composition and structure. *Science* **311**, 1419–1422 (2006).
15. N. Khawaja et al., Low-mass nitrogen-, oxygen-bearing, and aromatic compounds in Enceladean ice grains. *Mon. Not. R. Astron. Soc.* **489**, 5231–5243 (2019).
16. F. Postberg et al., Macromolecular organic compounds from the depths of Enceladus. *Nature* **558**, 564–568 (2018).
17. T. N. Chiesl et al., Enhanced amine and amino acid analysis using Pacific Blue and the Mars Organic Analyzer microchip capillary electrophoresis system. *Anal. Chem.* **81**, 2537–2544 (2009).
18. R. A. Mathies et al., Feasibility of detecting bioorganic compounds in Enceladus plumes with the Enceladus Organic Analyzer. *Astrobiology* **17**, 902–912 (2017).
19. P. A. Willis, J. S. Creamer, M. F. Mora, Implementation of microchip electrophoresis instrumentation for future spaceflight missions. *Anal. Bioanal. Chem.* **407**, 6939–6963 (2015).
20. M. Neveu et al., Returning samples from Enceladus for life detection. *Front. Astron. Space Sci.* **7**, 26 (2020).
21. M. Guzman et al., Collecting amino acids in the Enceladus plume. *Int. J. Astrobiol.* **18**, 47–59 (2019).
22. J. S. New et al., Characterizing organic particle impacts on inert metal surfaces: Foundations for capturing organic molecules during hypervelocity transits of Enceladus plumes. *Meteorit. Planet. Sci.* **55**, 465–479 (2020).
23. D. P. Glavin, J. P. Dworkin, S. A. Sandford, Detection of cometary amines in samples returned by Stardust. *Meteorit. Planet. Sci.* **43**, 399–413 (2008).
24. J. E. Elsila, D. P. Glavin, J. P. Dworkin, Cometary glycine detected in samples returned by Stardust. *Meteorit. Planet. Sci.* **44**, 1323–1330 (2009).
25. M. J. Burchell, M. J. Cole, J. A. M. McDonnell, J. C. Zarnecki, Hypervelocity impact studies using the 2 MV Van de Graaff accelerator and two-stage light gas gun of the University of Kent at Canterbury. *Meas. Sci. Technol.* **10**, 41–50 (1999).
26. R. Hibbert, M. J. Cole, M. C. Price, M. J. Burchell, The Hypervelocity Impact Facility at the University of Kent: Recent upgrades and specialized capabilities. *Procedia Eng.* **204**, 208–214 (2017).
27. J. S. New et al., Feasibility of Enceladus plume biosignature analysis: Successful capture of organic ice particles in hypervelocity impacts. *Meteorit. Planet. Sci.* **55**, 1936–1948 (2020).
28. Y. Dong, T. W. Hill, S. Ye, Characteristics of ice grains in the Enceladus plume from Cassini observations. *J. Geophys. Res. Space Phys.* **120**, 915–937 (2015).
29. B. Kazemi et al., Method for detecting and quantitating capture of organic molecules in hypervelocity impacts. *MethodsX* **8**, 101239 (2021).
30. M. Neveu, L. E. Hays, M. A. Voytek, M. H. New, M. D. Schulte, The ladder of life detection. *Astrobiology* **18**, 1375–1402 (2018).
31. K. Reh et al., "Enceladus Life Finder: The search for life in a habitable Moon," *2016 IEEE Aerospace Conference* (IEEE, Piscataway, NJ, 2016), pp. 1–8.
32. F. Postberg, J. Schmidt, J. Hillier, S. Kempf, R. Srama, A salt-water reservoir as the source of a compositionally stratified plume on Enceladus. *Nature* **474**, 620–622 (2011).
33. A. P. Ingersoll, S. P. Ewald, Decadal timescale variability of the Enceladus plumes inferred from Cassini images. *Icarus* **282**, 260–275 (2017).
34. M. M. Hedman et al., Spatial variations in the dust-to-gas ratio of Enceladus' plume. *Icarus* **305**, 123–138 (2018).
35. B. D. Teolis et al., Enceladus plume structure and time variability: Comparison of Cassini observations. *Astrobiology* **17**, 926–940 (2017).
36. M. M. Hedman et al., An observed correlation between plume activity and tidal stresses on Enceladus. *Nature* **500**, 182–184 (2013).
37. S. Kempf, U. Beckmann, J. Schmidt, How the Enceladus dust plume feeds Saturn's E ring. *Icarus* **206**, 446–457 (2010).
38. P. Gao, P. Kopparla, X. Zhang, A. P. Ingersoll, Aggregate particles in the plumes of Enceladus. *Icarus* **264**, 227–238 (2016).
39. C. C. Porco, L. Dones, C. Mitchell, Could it be snowing microbes on Enceladus? Assessing conditions in its plume and implications for future missions. *Astrobiology* **17**, 876–901 (2017).
40. , *K.P. Hand et al., Report of the Europa Lander Science Definition Team* (National Aeronautics and Space Administration, 2017), 1–264.
41. L. Rothschild, "Extremophiles: Defining the envelope for the search for life in the universe" in *Planetary Systems and the Origins of Life*, R. Pudritz, P. Higgs, J. Stone, Eds. (Cambridge University Press, 2007), pp. 113–1134.
42. B. C. Christner, G. Royston-Bisho, C. M. Foreman, Limnological conditions in subglacial lake Vostok, Antarctica. *Limnol. Oceanogr.* **51**, 2485–2501 (2006).
43. E. Kuhn et al., Brine assemblages of ultrasmall microbial cells within the ice cover of Lake Vida, Antarctica. *Appl. Environ. Microbiol.* **80**, 3687–3698 (2014).
44. Y. Shen et al., Bioavailable dissolved organic matter and biological hot spots during austral winter in Antarctic waters. *J. Geophys. Res. Oceans* **122**, 508–520 (2017).
45. J. P. Landers, *Handbook of Capillary and Microchip Electrophoresis and Associated Microtechniques* (CRC Press, 2007).
46. N. J. Dovichi, J. C. Martin, J. H. Jett, R. A. Keller, Attogram detection limit for aqueous dye samples by laser-induced fluorescence. *Science* **219**, 845–847 (1983).
47. K. Peck, L. Stryer, A. N. Glazer, R. A. Mathies, Single-molecule fluorescence detection: Autocorrelation criterion and experimental realization with phycoerythrin. *Proc. Natl. Acad. Sci. U.S.A.* **86**, 4087–4091 (1989).
48. V. A. Galievsky, A. S. Stasheuski, S. N. Krylov, "Getting the best sensitivity from on-capillary fluorescence detection in capillary electrophoresis"—A tutorial. *Anal. Chim. Acta* **935**, 58–81 (2016).
49. A. M. Skelley et al., Development and evaluation of a microdevice for amino acid biomarker detection and analysis on Mars. *Proc. Natl. Acad. Sci. U.S.A.* **102**, 1041–1046 (2005).
50. J. Kim, A. M. Stockton, E. C. Jensen, R. A. Mathies, Pneumatically actuated microvalve circuits for programmable automation of chemical and biochemical analysis. *Lab Chip* **16**, 812–819 (2016).
51. M. Golozar et al., Fabrication of high-quality glass microfluidic devices for bioanalytical and space flight applications. *MethodsX* **7**, 101043 (2020).
52. P. Tsou et al., LIFE: Life investigation for enceladus a sample return mission concept in search for evidence of life. *Astrobiology* **12**, 730–742 (2012).
53. L. Massarweh, P. Cappuccio, *On the Restricted 3-Body Problem for the Saturn-Enceladus System: Mission Geometry & Orbit Design for Plume Sampling Missions* (AIAA SciTech Forum, 2020).
54. C. J. Hansen et al., The composition and structure of Enceladus' plume from the complete set of Cassini UVIS occultation observations. *Icarus* **344**, 113461 (2020).
55. R. A. Mathies, M. G. A. L. Butterworth, J. McCauley, J. S. New, "High/hyper-velocity particle capture and impact method and apparatus." International Patent Application PCT number WO 2020/131342 A2 (2020).
56. M. D. Abràmoff, P. J. Magalhães, S. J. Ram, Image processing with ImageJ. *Biophoton. Int.* **11**, 36–42 (2004).

**6 of 6** | **PNAS**
https://doi.org/10.1073/pnas.2106197118

**New et al.**
Quantitative evaluation of the feasibility of sampling the ice plumes at Enceladus for biomarkers of extraterrestrial life